

# NUMERICAL MODELING OF VERY THIN DIELECTRIC MATERIALS

Except where reference is made to the work of others, the work described in this thesis is my own or was done in collaboration with my advisory committee. This thesis does not include proprietary or classified information.

---

Tyler Norton Killian

Certificate of Approval:

---

Michael E. Baginski  
Associate Professor  
Electrical Engineering

---

Sadasiva M. Rao, Chair  
Professor  
Electrical Engineering

---

Lloyd S. Riggs  
Professor  
Electrical Engineering

---

Joe F. Pittman  
Interim Dean  
Graduate School

NUMERICAL MODELING OF VERY THIN DIELECTRIC MATERIALS

Tyler Norton Killian

A Thesis

Submitted to

the Graduate Faculty of

Auburn University

in Partial Fulfillment of the

Requirements for the

Degree of

Master of Science

Auburn, Alabama

August 9, 2008

# NUMERICAL MODELING OF VERY THIN DIELECTRIC MATERIALS

Tyler Norton Killian

Permission is granted to Auburn University to make copies of this thesis at its discretion, upon the request of individuals or institutions and at their expense. The author reserves all publication rights.

---

Signature of Author

---

Date of Graduation

## VITA

Tyler N. Killian, son of John and Robin Killian, was born on March 9, 1983, in Gadsden, Alabama. He attended high school at Sand Rock High School in Sand Rock, Alabama and graduated in 2001. He graduated with a Bachelor of Electrical Engineering degree from Auburn University, Auburn, Alabama in 2005. In Fall 2005, he entered graduate school at Auburn University and plans to obtain a Ph.D. in Electrical Engineering.

THESIS ABSTRACT

NUMERICAL MODELING OF VERY THIN DIELECTRIC MATERIALS

Tyler Norton Killian

Master of Science, August 9, 2008  
(B.E.E., Auburn University, 2005)

46 Typed Pages

Directed by Sadasiva M. Rao

In this work, a Method of Moments (MoM) formulation is presented for the numerical solution of very thin dielectric materials in the frequency domain. The dielectric material is represented by a triangular mesh and a parameter controlling the thickness of the dielectric. The triangular mesh can represent bodies with arbitrary curvature and results in significantly fewer unknowns than volume formulations.

The dielectric material is first replaced with an equivalent set of currents. An integral equation is then developed to relate the currents in the dielectric material to an incident excitation wave. Currents flowing tangentially to the surface of the dielectric are represented by a set of RWG functions and half-RWG functions at the boundary edges in order to account for charges at the edge of the dielectric. Currents normal to the surface are modeled by pulse functions which also account for surface charges on the dielectric sheet. The MoM procedure is then applied resulting in a linear system which can be easily solved by matrix inversion.

Finally, the dielectric is coupled with a perfect electrical conductor solution allowing us to solve systems involving both conducting and thin dielectric materials.

Furthermore, the similarity between the dielectric and conductor basis functions allows one to easily add support for conductors once the dielectric code has been implemented or vice versa.

## ACKNOWLEDGMENTS

To the author's parents, he expresses his appreciation for their love and encouragement throughout life.

To his advisor, Dr. Sadasiva M. Rao, he thanks for his patience and top-notch guidance. His expertise has been invaluable for this work.

To Dr. Michael Baginski, he thanks for his encouragement and interesting technical discussions.

To the NASA Langley Research Center, he expresses his appreciation for the fellowship which made this work possible.

Style manual or journal used Journal of Approximation Theory (together with the style known as “aums”). Bibliography follows van Leunen’s *A Handbook for Scholars*.

Computer software used The document preparation package T<sub>E</sub>X (specifically L<sub>A</sub>T<sub>E</sub>X) together with the departmental style-file `aums.sty`.



## TABLE OF CONTENTS

LIST OF FIGURES	x
1 INTRODUCTION	1
1.1 Background and Objectives . . . . .	1
1.2 Outline . . . . .	3
2 THIN DIELECTRIC	5
2.1 Electric Field Integral Equation - EFIE . . . . .	6
2.2 Current Expansion . . . . .	8
2.3 Testing Procedure . . . . .	12
2.4 Numerical Results . . . . .	16
3 COMBINED PEC/THIN DIELECTRIC	21
3.1 Electric Field Integral Equation - EFIE . . . . .	21
3.2 Current Expansion . . . . .	23
3.3 Testing Procedure . . . . .	24
3.4 Numerical Results . . . . .	27
4 CONCLUSIONS	29
BIBLIOGRAPHY	31
A NUMERICAL RESULTS	32
A.1 RCS . . . . .	32
A.2 Antenna Input Impedance . . . . .	33
A.3 A Note On Dielectric Meshing Requirements . . . . .	34

## LIST OF FIGURES

1.1	Illustration of dielectric sheet with thickness $\tau$ . Each triangle can be assigned a relative permittivity. . . . .	3
2.1	Thin dielectric sheet with incident field $\mathbf{E}^i$ and observation point $\mathbf{r}$ . . . . .	6
2.2	Basis for tangential currents in dielectric. . . . .	11
2.3	Basis for normal currents in dielectric. . . . .	11
2.4	Quantities used when tangential basis functions overlap. . . . .	14
2.5	Bistatic RCS at $\phi = 0^0$ by 0.5 m x 0.02 m x 0.001 m dielectric strip with $\varepsilon_r = 2.6$ and an incident wave from $(\theta, \phi) = (180^0, 0^0)$ at 0.2 Ghz with $E_\theta = \eta$ . . . . .	17
2.6	Bistatic RCS at $\phi = 0^0$ by 0.5 m x 0.02 m x 0.001 m dielectric strip with $\varepsilon_r = 2.6$ and an incident wave from $(\theta, \phi) = (180^0, 90^0)$ at 0.2 Ghz with $E_\theta = \eta$ . . . . .	17
2.7	Inhomogeneous dielectric square of dimension 1.0 m x 1.0 m x 0.02 m. . . . .	18
2.8	Bistatic RCS at $\phi = 0^0$ by 1.0 m x 1.0 m x 0.02 m inhomogeneous square with $\varepsilon_r = 2.2, 4.1, 5.7, 7.3$ and an incident wave from $(\theta, \phi) = (120^0, 30^0)$ at 0.1 Ghz with $E_\theta = -\eta$ . . . . .	18
2.9	Bistatic RCS at $\phi = 0^0$ by a dielectric sphere with radius = 1.0 m and thickness = 0.05 m with $\varepsilon_r = 2.6$ and an incident wave from $(\theta, \phi) = (180^0, 0^0)$ at 0.2 Ghz with $E_\theta = \eta$ . . . . .	19
2.10	Bistatic RCS at $\phi = 90^0$ by a dielectric sphere with radius = 1.0 m and thickness = 0.05 m with $\varepsilon_r = 2.6$ and an incident wave from $(\theta, \phi) = (180^0, 0^0)$ at 0.2 Ghz with $E_\theta = \eta$ . . . . .	19
2.11	Monostatic RCS at $\phi = 0^0$ by a homogeneous dielectric square with dimension 10.16 cm x 10.16 cm x 0.00635 cm with $\varepsilon_r = 4$ and an 2.4 GHz incident wave with $E_\phi = \eta$ (TE polarization) . . . . .	20

2.12	Monostatic RCS at $\phi = 0^0$ by a homogeneous dielectric square with dimension 10.16 cm x 10.16 cm x 0.00635 cm with $\epsilon_r = 4$ and an 2.4 GHz incident wave with $H_\phi = 1$ (TM polarization) . . . . .	20
3.1	Geometry for patch antenna. . . . .	28
3.2	Return loss by patch antenna with homogeneous dielectric with $\epsilon_r = 5.7$ and thickness = 0.15 in. The ground plane has dimensions 3.0 in x 2.4 in. The patch has dimensions 1.8 in x 1.2 in. . . . .	28

## CHAPTER 1

### INTRODUCTION

#### 1.1 Background and Objectives

Thin dielectrics appear in various practical situations such as microstrip antennas, radomes, and aircraft built with composite materials. Typical numerical formulations based on either surface or volume integral equations suffer from large numbers of unknowns as well as meshing difficulties. In this work, a Method of Moments (MoM) [4] solution is presented which models a thin dielectric with constant thickness as a two-dimensional sheet with a triangular mesh. This technique not only increases the numerical efficiency, but also eases the meshing process.

Using the equivalence principle, the dielectric is replaced by an equivalent set of currents. Since the dielectric is thin, equivalent currents both tangential and normal to the surface can be assumed constant throughout the thickness of the dielectric. These currents are then represented by two sets of basis functions. A set of RWG [1] bases represents tangential currents in the dielectric. In order to account for charge at the outer edges of the dielectric, a half-RWG basis is used so the current flowing into the edge is non-zero. Pulse functions represent currents flowing normal to the surface. The inclusion of this normal component ensures accuracy for problems involving grazing incident waves. Furthermore, it allows us to model problems where the current is dominated by the normal component. For example, a conductor coated with a thin dielectric will have a near-zero electric field near the surface of the conductor and

consequently very little tangential current in the dielectric. Microstrip problems with thin dielectric substrates also have a strong field in the normal direction. Allowing the pulse functions to extend to the surface of the dielectric accounts for any charge accumulating on the surface. Although the normal component can be modeled as an equivalent magnetic current as in [6], the electric current equivalent seems to be more intuitive. Also, since we replace the dielectric with a set of currents in free space, we no longer have to explicitly enforce boundary conditions for the fields at the boundary of the dielectric - they are satisfied automatically. This is one advantage over the D-field formulation as in [2] and [7]. Furthermore, in the current equivalent model, the boundary conditions between mesh elements are enforced directly in the basis function.

The dielectric sheet is meshed by a two-dimensional triangular mesh along with a single parameter to control the thickness of the dielectric. Triangular meshing makes it possible to accurately model complex geometries since triangular patches can easily conform to curves and support refinement where a denser mesh is required. Furthermore, typical volume formulations, such as [8], involve using a three-dimensional tetrahedral mesh. Triangular meshes are much easier to generate especially for complex geometries. For very thin dielectrics, tetrahedral elements may also be severely skewed causing numerical errors and meshing difficulty. Finally, both homogeneous and heterogeneous dielectrics can be simulated by assigning a relative permittivity to each triangle as illustrated in Figure 1.1.

Finally, the dielectric code can be easily integrated with existing moment codes for simulating conductors. Due to the thin sheet approximation, many of the moment

terms are similar to those found in PEC formulations using RWG functions. Consequently, one can add support for combined conductor and dielectric problems with little extra programming effort. The resulting code supports microstrip problems with thin dielectrics as well as conductors with thin material coatings.

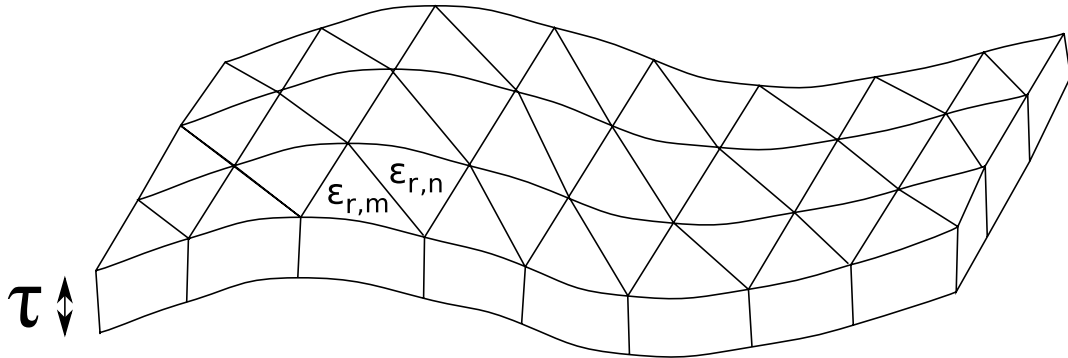


Figure 1.1: Illustration of dielectric sheet with thickness  $\tau$ . Each triangle can be assigned a relative permittivity.

## 1.2 Outline

In Chapter 2 we develop the integral equation for the thin dielectric surface. The MoM code is then developed through a straightforward expansion and testing process. This results in a linear system which can be easily solved by matrix inversion. Numerical results are then presented to verify the accuracy of the method.

The combined PEC/thin dielectric code is developed in Chapter 3 by expanding the dielectric code. A pair of coupled integral equations is used to generate a new linear system. The dielectric portion is seen to be a submatrix in the new system. Also, due to the choice of basis functions and the surface formulation used for the

dielectric, the conductor coupling terms are compared to those for the dielectric in order to aid the programming process.

## CHAPTER 2

### THIN DIELECTRIC

In this chapter, we develop the integral equation formulation and the MoM procedure for the thin dielectric. In section 2.1, we use the current equivalent formulation to replace the dielectric material with a set of currents in free space. We then develop an integral equation which relates the currents to the incident electric field providing us with the governing equation for the system.

In section 2.2 we replace the currents with two sets of basis functions. One set approximates the currents tangential to the surface of the dielectric while the other set represents currents flowing normal to the surface. We then expand the governing equation in terms of these functions. Due to the dielectric being very thin, we can reduce all the volume integrals to surface integrals.

Next, in section 2.3, we generate a matrix system by testing the integral equation using the Galerkin method. This system can be solved by a standard linear equation solver providing us with the currents in the dielectric.



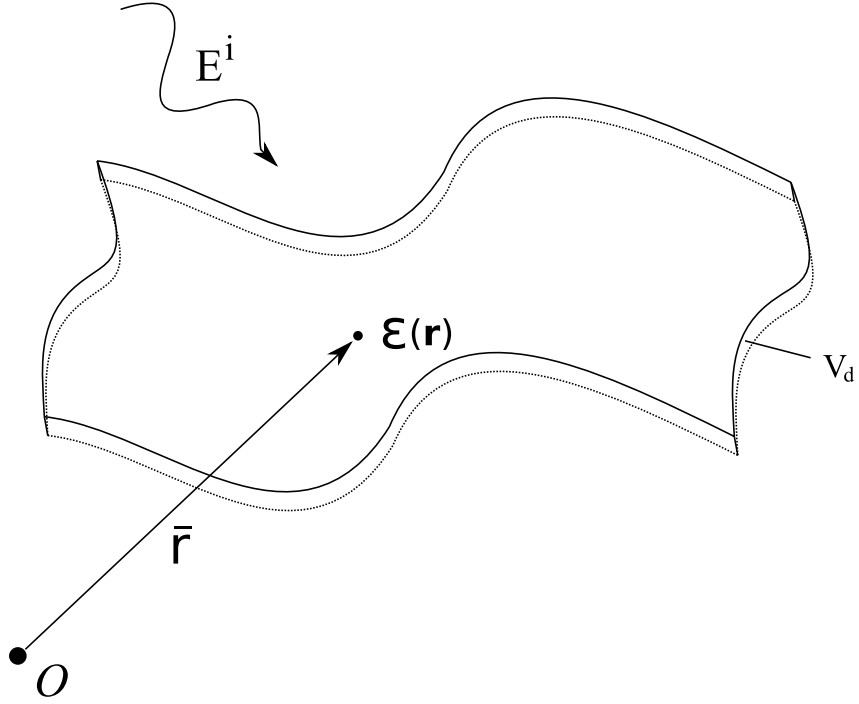


Figure 2.1: Thin dielectric sheet with incident field  $\mathbf{E}^i$  and observation point  $\mathbf{r}$ .

## 2.1 Electric Field Integral Equation - EFIE

Consider a dielectric sheet illuminated by an incident electric field as shown in Figure 2.1. First, we replace the dielectric structure with an equivalent set of currents. If  $\epsilon_r(\mathbf{r})$  is the relative permittivity at a point  $\mathbf{r}$  in the dielectric then the equivalent current  $\mathbf{J}(\mathbf{r})$  is related to the total electric field  $\mathbf{E}^t(\mathbf{r})$  by:

$$\begin{aligned}
 \mathbf{J}(\mathbf{r}) &= j\omega\epsilon_o(\epsilon_r(\mathbf{r}) - 1)\mathbf{E}^t(\mathbf{r}) \\
 &= \Omega(\mathbf{r})\mathbf{E}^t(\mathbf{r}) \text{ where } \Omega(\mathbf{r}) = j\omega\epsilon_o(\epsilon_r(\mathbf{r}) - 1)
 \end{aligned} \tag{2.1}$$

Here,  $\epsilon_o$  is the permittivity of free space and  $\omega = 2\pi f$  where  $f$  is the frequency of interest. Equation (2.1) effectively acts as the boundary condition for the electric field. The total electric field is the sum of the incident field  $\mathbf{E}^i$  and the scattered field  $\mathbf{E}^s$ :

$$\mathbf{E}^t(\mathbf{r}) = \mathbf{E}^i(\mathbf{r}) + \mathbf{E}^s(\mathbf{r}) \quad (2.2)$$

The scattered field is related to the current by:

$$\mathbf{E}^s(\mathbf{r}) = -j\omega\mathbf{A}(\mathbf{r}) - \nabla\Phi(\mathbf{r}) \quad (2.3)$$

where the magnetic vector potential is

$$\mathbf{A}(\mathbf{r}) = \mu \int_{V_d} \mathbf{J}(\mathbf{r}')G(\mathbf{r}, \mathbf{r}')dv' \quad (2.4)$$

and the scalar potential is given by:

$$\Phi(\mathbf{r}) = \frac{-1}{j\omega\epsilon} \int_{V_d} \nabla \cdot \mathbf{J}(\mathbf{r}')G(\mathbf{r}, \mathbf{r}')dv' \quad (2.5)$$

where  $V_d$  is the dielectric volume and

$$G(\mathbf{r}, \mathbf{r}') = \frac{e^{-jkR}}{4\pi R} \text{ and } R = |\mathbf{r} - \mathbf{r}'| \quad (2.6)$$

Substituting for the total electric field and rewriting the scattered field in terms of  $\mathbf{A}$  and  $\Phi$  provides us with the governing equation:

$$\mathbf{E}^i(\mathbf{r}) = \frac{\mathbf{J}}{\Omega}(\mathbf{r}) + j\omega\mathbf{A}(\mathbf{r}) + \nabla\Phi(\mathbf{r}), \mathbf{r} \in V_d \quad (2.7)$$

This equation is suitable for use in the MoM formulation.

## 2.2 Current Expansion

The total current can be broken up into a tangential part  $\mathbf{J}_p$  and a normal part  $\mathbf{J}_q$ . Each current component is then approximated by a set of basis functions. Let  $\mathbf{P}_n$  for  $n = 1, \dots, N_p$  and  $\mathbf{Q}_n$  for  $n = 1, \dots, N_q$  be the basis for the tangential and normal components of the current. Then

$$\mathbf{J} = \mathbf{J}_p + \mathbf{J}_q \cong \sum_{n=1}^{N_p} \alpha_n \mathbf{P}_n + \sum_{n=1}^{N_q} \beta_n \mathbf{Q}_n \quad (2.8)$$

Since the mesh is triangular, we can use a slightly modified RWG basis for the tangential current. For nonboundary edges, the definition is similar to that used for PEC surfaces [1]:

$$\mathbf{P}_{n,nonboundary}(\mathbf{r}) = \begin{cases} \left( \frac{\varepsilon_{r,n}^+ - 1}{\varepsilon_{r,n}^+} \right) \frac{l_n}{2A_n^+} \rho_n^+, & \mathbf{r} \in T_n^+ \\ \left( \frac{\varepsilon_{r,n}^- - 1}{\varepsilon_{r,n}^-} \right) \frac{l_n}{2A_n^-} \rho_n^-, & \mathbf{r} \in T_n^- \\ 0, & \text{otherwise} \end{cases} \quad (2.9)$$

with the exception that each side is multiplied by  $\left( \frac{\varepsilon_r^\pm - 1}{\varepsilon_r^\pm} \right)$  to compensate for varying relative permittivities. This multiplier ensures that the electric flux density  $D$  normal to the edge corresponding to the basis is continuous. In terms of the current equivalent model, this means charge will collect between two adjacent triangles with different permittivities. The quantities are shown in Figure 2.2. Also, in the dielectric case, the basis is defined on a pair of prisms rather than a pair of triangles. Since the dielectric

is thin, the tangential current is assumed constant throughout the thickness of the dielectric. Also, since we need to be able to support charge accumulating at the edge of the dielectric, we use a half-basis for boundary edges:

$$\mathbf{P}_{n,boundary}(\mathbf{r}) = \begin{cases} \left( \frac{\varepsilon_{r,n}-1}{\varepsilon_{r,n}} \right) \frac{l_n}{2A_n} \rho_n, & \mathbf{r} \in T_n \\ 0, & \text{otherwise} \end{cases} \quad (2.10)$$

This basis is the same as the RWG basis with the exception that it is defined on a single triangle.

For the current component normal to the surface, a pulse basis is used:

$$Q_n(\mathbf{r}) = \begin{cases} \hat{n}_n, & \mathbf{r} \in T_n \\ 0, & \text{otherwise} \end{cases} \quad (2.11)$$

where  $\hat{n}_n$  is a unit vector normal to the surface as illustrated in Figure 2.3. The pulse extends to each side of the dielectric sheet allowing for any charge accumulation on the surface.

Substituting (2.8) into (2.7) we get:

$$\mathbf{E}^i = \sum_{n=1}^{N_p} \alpha_n \left( \frac{\mathbf{P}_n}{\Omega} + j\omega \mathbf{A}_{p,n} + \nabla \Phi_{p,n} \right) + \sum_{n=1}^{N_q} \beta_n \left( \frac{\mathbf{Q}_n}{\Omega} + j\omega \mathbf{A}_{q,n} + \nabla \Phi_{q,n} \right) \quad (2.12)$$

where

$$\mathbf{A}_{p,n}(\mathbf{r}) = \mu \int_{V_n} \mathbf{P}_n(\mathbf{r}') G(\mathbf{r}, \mathbf{r}') dv' \quad (2.13)$$

$$\Phi_{p,n}(\mathbf{r}) = \frac{-1}{j\omega\varepsilon} \int_{V_n} \nabla \cdot \mathbf{P}_n(\mathbf{r}') G(\mathbf{r}, \mathbf{r}') dv' \quad (2.14)$$

$$\mathbf{A}_{q,n}(\mathbf{r}) = \mu \int_{V_n} \mathbf{Q}_n(\mathbf{r}') G(\mathbf{r}, \mathbf{r}') dv' \quad (2.15)$$

$$\Phi_{q,n}(\mathbf{r}) = \frac{-1}{j\omega\epsilon} \int_{V_n} \nabla \cdot \mathbf{Q}_n(\mathbf{r}') G(\mathbf{r}, \mathbf{r}') dv' \quad (2.16)$$

We let  $dv = dSdn$  where  $n$  is positive in the direction of  $\hat{n}_n$ . Since the dielectric is thin, we can approximate the integrands in (2.13), (2.14), and (2.15) as being constant throughout the thickness of the dielectric. Also, we note that  $\nabla \cdot \mathbf{Q}_n = -\delta(n = \tau) + \delta(n = 0)$ . We can then rewrite (2.13-2.16) as

$$\mathbf{A}_{p,n}(\mathbf{r}) = \mu\tau \int_{S_n} \mathbf{P}_n(\mathbf{r}') G(\mathbf{r}, \mathbf{r}') dS' \quad (2.17)$$

$$\Phi_{p,n}(\mathbf{r}) = \frac{-\tau}{j\omega\epsilon} \int_{S_n} \nabla \cdot \mathbf{P}_n(\mathbf{r}') G(\mathbf{r}, \mathbf{r}') dS' \quad (2.18)$$

$$\mathbf{A}_{q,n}(\mathbf{r}) = \mu\tau \int_{S_n} \mathbf{Q}_n(\mathbf{r}') G(\mathbf{r}, \mathbf{r}') dS' \quad (2.19)$$

$$\Phi_{q,n}(\mathbf{r}) = \frac{1}{j\omega\epsilon} \left[ \int_{S_n^+} G(\mathbf{r}, \mathbf{r}') dS' - \int_{S_n^-} G(\mathbf{r}, \mathbf{r}') dS' \right] \quad (2.20)$$

where  $S_n^+$  is the top surface (pointed to by  $\hat{n}_n$ ) and  $S_n^-$  is the bottom surface of  $T_n$ .  $S_n$  is the surface located at the center of the prism element. Thus, all integrals are reduced to surface integrals rather than volume integrals.

Some useful quantities are the following:

$$\nabla \cdot \mathbf{P}_n = \begin{cases} \left( \frac{\epsilon_{r,n}^+ - 1}{\epsilon_{r,n}^+} \right) \frac{l_n}{A_n^+}, & \mathbf{r} \in T_n^+ \\ \left( \frac{\epsilon_{r,n}^- - 1}{\epsilon_{r,n}^-} \right) \frac{-l_n}{A_n^-}, & \mathbf{r} \in T_n^- \\ 0, & \text{otherwise} \end{cases} \quad (2.21)$$

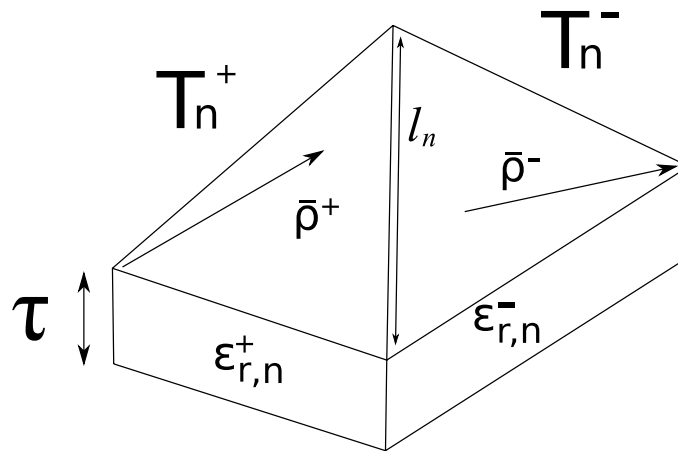


Figure 2.2: Basis for tangential currents in dielectric.

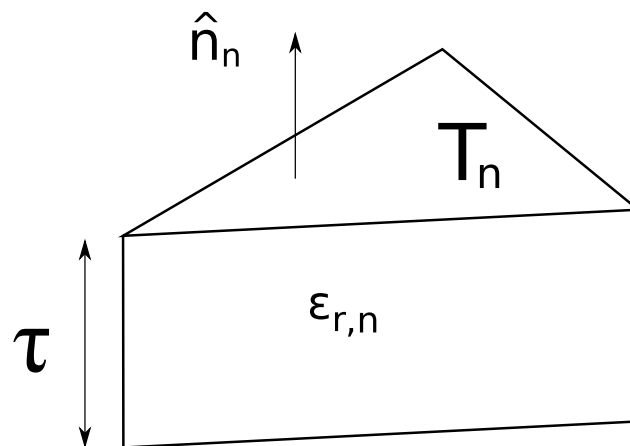


Figure 2.3: Basis for normal currents in dielectric.

To determine the surface charge on the dielectric we apply the continuity equation  $\nabla \cdot \mathbf{J} = -j\omega\sigma_s$  to get:

$$\sigma_{s,n} = \pm \frac{\alpha_n}{j\omega} \left( \frac{\varepsilon_{r,n} - 1}{\varepsilon_{r,n}} \right) \quad (2.22)$$

for a half-rwg function at a boundary edge where the plus sign is taken for a basis directed out of the triangle and the minus sign if the basis is directed into the triangle.

For the top and bottom surface we have

$$\sigma_{s,n} = \pm \frac{\beta_n}{j\omega} \quad (2.23)$$

for the pulse functions where the positive sign is taken for the side pointed to by  $\hat{n}_n$  and the negative sign taken otherwise. Note that equal charges with opposite signs accumulate on the top and bottom of the dielectric sheet.

### 2.3 Testing Procedure

We use Galerkin's procedure to generate a set of linear equations. To do this we test both sides of (2.12) with each of the previously defined basis functions using the following inner product:

$$\langle \mathbf{f}, \mathbf{g} \rangle \equiv \int \mathbf{f} \cdot \mathbf{g} dv \quad (2.24)$$

This gives us a matrix equation of the form:

$$\begin{bmatrix} Z_{pp} & Z_{pq} \\ Z_{qp} & Z_{qq} \end{bmatrix} \begin{bmatrix} I_p \\ I_q \end{bmatrix} = \begin{bmatrix} V_p \\ V_q \end{bmatrix} \quad (2.25)$$

The submatrices  $Z_{pp}$ ,  $Z_{qq}$ ,  $Z_{pq}$ , and  $Z_{qp}$  represent the coupling between the basis functions.  $V_p$  and  $V_q$  are the excitations from the tangential and normal incident fields.  $I_p$  and  $I_q$  are the values to be solved for representing the magnitudes of the expansion functions.

The coupling terms are given by:

$$Z_{pp,mn} = \frac{1}{\Omega} \langle \mathbf{P}_n, \mathbf{P}_m \rangle + j\omega \langle \mathbf{A}_{p,n}, \mathbf{P}_m \rangle + \langle \nabla \Phi_{p,n}, \mathbf{P}_m \rangle \quad (2.26)$$

$$Z_{pq,mn} = j\omega \langle \mathbf{A}_{q,n}, \mathbf{P}_m \rangle + \langle \nabla \Phi_{q,n}, \mathbf{P}_m \rangle \quad (2.27)$$

$$Z_{qp,mn} = j\omega \langle \mathbf{A}_{p,n}, \mathbf{Q}_m \rangle + \langle \nabla \Phi_{p,n}, \mathbf{Q}_m \rangle \quad (2.28)$$

$$Z_{qq,mn} = \frac{1}{\Omega} \langle \mathbf{Q}_n, \mathbf{Q}_m \rangle + j\omega \langle \mathbf{A}_{q,n}, \mathbf{Q}_m \rangle + \langle \nabla \Phi_{q,n}, \mathbf{Q}_m \rangle \quad (2.29)$$

and the excitation vectors by:

$$V_{p,m} = \langle \mathbf{E}^i, \mathbf{P}_m \rangle \quad (2.30)$$

$$V_{q,m} = \langle \mathbf{E}^i, \mathbf{Q}_m \rangle \quad (2.31)$$

The testing terms are evaluated in the following. If  $\mathbf{P}_m$  and  $\mathbf{P}_n$  overlap on some triangle  $T$  with permittivity  $\varepsilon_r$ , let  $\mathbf{r}^{ct}$ ,  $\mathbf{r}_1$ ,  $\mathbf{r}_2$ , and  $\mathbf{r}_3$  represent the position vectors of the centroid of  $T$  and each of the three vertices as shown in Figure 2.4.

$$\begin{aligned} \langle \mathbf{P}_n, \mathbf{P}_m \rangle_T &= \pm \frac{l_m l_n \tau}{4A_m} \left( \frac{\varepsilon_r - 1}{\varepsilon_r} \right)^2 \left[ \frac{3|\mathbf{r}^{ct}|^2}{4} + \frac{|\mathbf{r}_1|^2 + |\mathbf{r}_2|^2 + |\mathbf{r}_3|^2}{12} \right. \\ &\quad \left. - (\mathbf{r}_m + \mathbf{r}_n) \cdot \mathbf{r}^{ct} + \mathbf{r}_m \cdot \mathbf{r}_n \right] \end{aligned} \quad (2.32)$$



where  $\mathbf{r}_m$  and  $\mathbf{r}_n$  are the position vectors corresponding to vertices associated with  $\mathbf{P}_m$  and  $\mathbf{P}_n$ . If  $m = n$  and  $\mathbf{P}_m$  is associated with a nonboundary edge, then both  $T_m^+$  and  $T_m^-$  will contribute to  $\langle \mathbf{P}_n, \mathbf{P}_m \rangle$ . Also note that the sign is positive if both bases are directed into or out of  $T$ , and is negative otherwise [5].

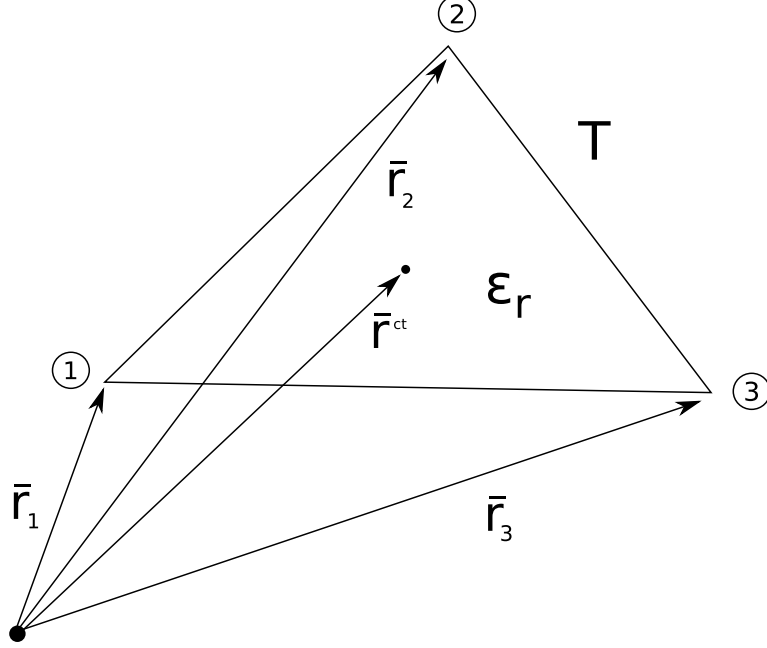


Figure 2.4: Quantities used when tangential basis functions overlap.

The testing terms for the RWG functions are similar to those for the PEC solution in [1] with the exception that they are multiplied by  $\tau$  to compensate for the thickness of the dielectric.

$$\left\langle \left\{ \begin{array}{c} \mathbf{E}^i \\ \mathbf{A}_{p/q,n} \end{array} \right\}, \mathbf{P}_m \right\rangle = \frac{l_m}{2} \tau \left[ \left( \frac{\epsilon_{r,m}^+ - 1}{\epsilon_{r,m}^+} \right) \left\{ \begin{array}{c} \mathbf{E}^i(\mathbf{r}_m^{ct+}) \\ \mathbf{A}_{p/q,n}(\mathbf{r}_m^{ct+}) \end{array} \right\} \cdot \rho_m^{ct+} \right. \\ \left. + \left( \frac{\epsilon_{r,m}^- - 1}{\epsilon_{r,m}^-} \right) \left\{ \begin{array}{c} \mathbf{E}^i(\mathbf{r}_m^{ct-}) \\ \mathbf{A}_{p/q,n}(\mathbf{r}_m^{ct-}) \end{array} \right\} \cdot \rho_m^{ct-} \right] \quad (2.33)$$

$$\langle \nabla \Phi_{p/q,n}, \mathbf{P}_m \rangle = -l_m \tau \left[ \left( \frac{\varepsilon_{r,m}^+ - 1}{\varepsilon_{r,m}^+} \right) \Phi_{p/q,n}(\mathbf{r}_m^{ct+}) - \left( \frac{\varepsilon_{r,m}^- - 1}{\varepsilon_{r,m}^-} \right) \Phi_{p/q,n}(\mathbf{r}_m^{ct-}) \right] \quad (2.34)$$

where  $\mathbf{r}_m^{ct+}$  and  $\mathbf{r}_m^{ct-}$  are the centroids of  $T_m^+$  and  $T_m^-$ . If  $\mathbf{P}_m$  is a half-basis, then the first summation terms in (2.33) and (2.34) are used if the basis is directed out of  $T_m$  and the second terms are used otherwise.

The testing terms for the pulse functions are as follows:

$$\langle \mathbf{Q}_n, \mathbf{Q}_m \rangle = \begin{cases} \frac{\tau A_m}{\Omega}, & \text{if } n = m \\ 0, & \text{otherwise} \end{cases} \quad (2.35)$$

$$\langle \mathbf{A}_{p/q,n}, \mathbf{Q}_m \rangle = \tau A_m \mathbf{A}_{p/q,n}(\mathbf{r}_m^{ct}) \cdot \hat{n}_m \quad (2.36)$$

$$\langle \nabla \Phi_{p/q,n}, \mathbf{Q}_m \rangle = \tau A_m \left( \frac{\Phi_{p/q,n}(\mathbf{r}_m^{ct} + 0.25\tau \hat{n}_m) - \Phi_{p/q,n}(\mathbf{r}_m^{ct} - 0.25\tau \hat{n}_m)}{0.5\tau} \right) \quad (2.37)$$

The term (2.37) comes from the fact that  $\nabla \Phi \cdot \mathbf{Q}_m = \frac{\partial \Phi}{\partial n}$ . This derivative is approximated at the centroid of  $T_m$  and is assumed constant throughout the prism volume.

At this point, a MoM formulation has been developed to handle both homogeneous and heterogeneous thin dielectric sheets. In the next chapter, this code is expanded to include arbitrary conductors as well.

## 2.4 Numerical Results

In this section, numerical results are presented to demonstrate the accuracy of the dielectric code. In Figures 2.5 and 2.6 a bistatic RCS is presented for a 0.5 m x 0.02 m x 0.001 m homogeneous rectangular strip with  $\epsilon_r = 2.6$ . The incident wave is directed perpendicular to the strip surface with the electric field oriented horizontally in Figure 2.5 and vertically in Figure 2.6. The results are compared with those found in [2].

In Figure 2.8 a bistatic RCS is given for an inhomogeneous square plate with dimensions 1.0 m x 1.0 m x 0.02 m. The plate is divided up into four equally sized smaller squares and each is assigned a different  $\epsilon_r$  as shown in Figure 2.7. This plate is illuminated with a 0.1 GHz incident wave from  $(\theta, \phi) = (120^\circ, 30^\circ)$ . The values are compared to those in [2] and are found to be in agreement.

Figures 2.9 and 2.10 show the bistatic RCS from a spherical shell with a radius of 1 m and thickness of 0.05 m. The dielectric is homogeneous with  $\epsilon_r = 2.6$ . The excitation is a 0.2 GHz incident wave at  $(\theta, \phi) = (180^\circ, 0^\circ)$ . Figure 2.9 shows the RCS at  $\phi = 0^\circ$  and Figure 2.10 gives the result at  $\phi = 90^\circ$ . The results are also compared to those in [2].

Figures 2.11 and 2.12 show the monostatic RCS at  $\phi = 0^\circ$  for a square plate with dimensions 10.16 cm x 10.16 cm x 0.00635 cm. The dielectric is homogeneous with  $\epsilon_r = 4$ . The incident wave has a frequency of 2.4 GHz. Figure 2.11 shows the RCS for a TE polarized wave. Figure 2.12 shows the TM case. The results are compared with those found in [7].

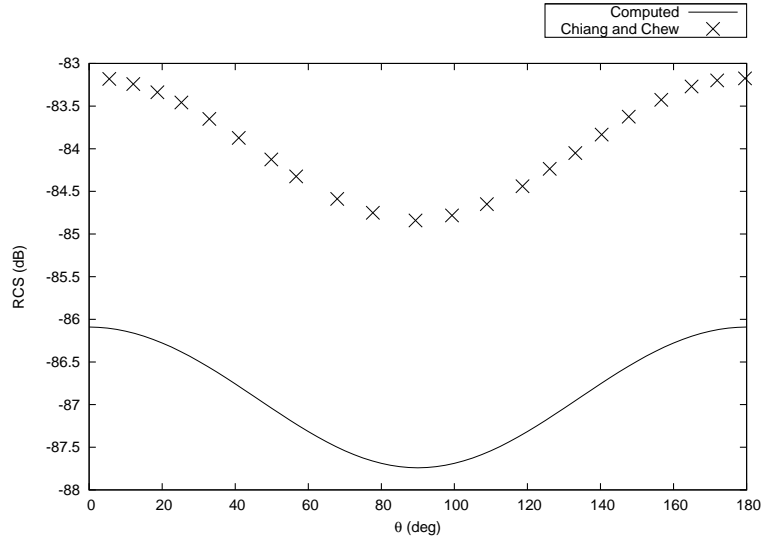


Figure 2.5: Bistatic RCS at  $\phi = 0^0$  by 0.5 m x 0.02 m x 0.001 m dielectric strip with  $\epsilon_r = 2.6$  and an incident wave from  $(\theta, \phi) = (180^0, 0^0)$  at 0.2 Ghz with  $E_\theta = \eta$

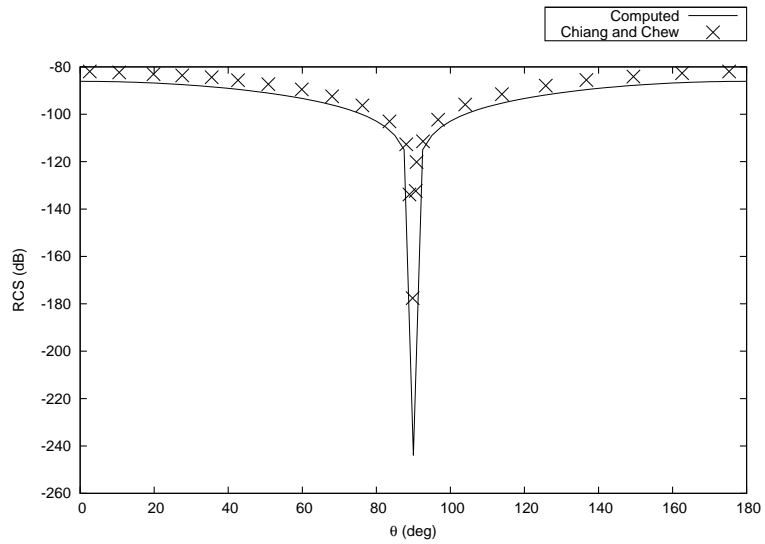


Figure 2.6: Bistatic RCS at  $\phi = 0^0$  by 0.5 m x 0.02 m x 0.001 m dielectric strip with  $\epsilon_r = 2.6$  and an incident wave from  $(\theta, \phi) = (180^0, 90^0)$  at 0.2 Ghz with  $E_\theta = \eta$

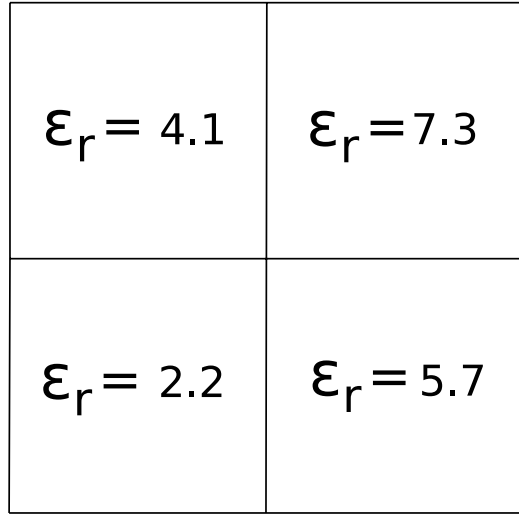


Figure 2.7: Inhomogeneous dielectric square of dimension 1.0 m x 1.0 m x 0.02 m.

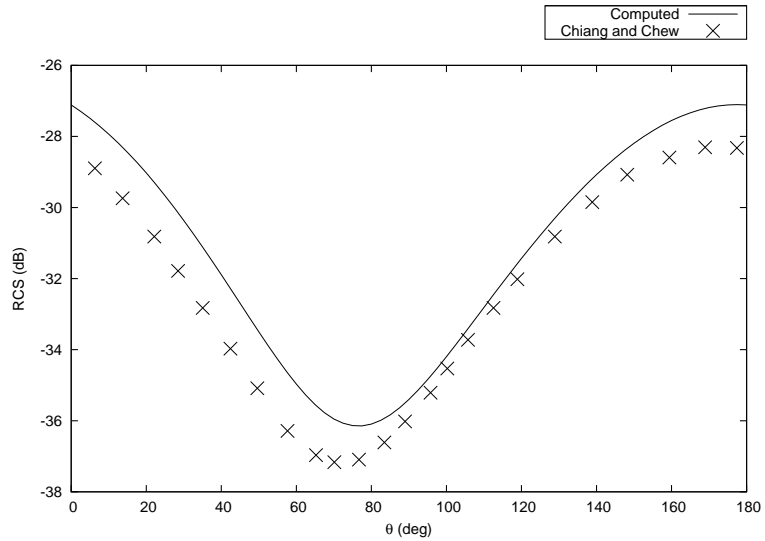


Figure 2.8: Bistatic RCS at  $\phi = 0^0$  by 1.0 m x 1.0 m x 0.02 m inhomogeneous square with  $\epsilon_r = 2.2, 4.1, 5.7, 7.3$  and an incident wave from  $(\theta, \phi) = (120^0, 30^0)$  at 0.1 Ghz with  $E_\theta = -\eta$

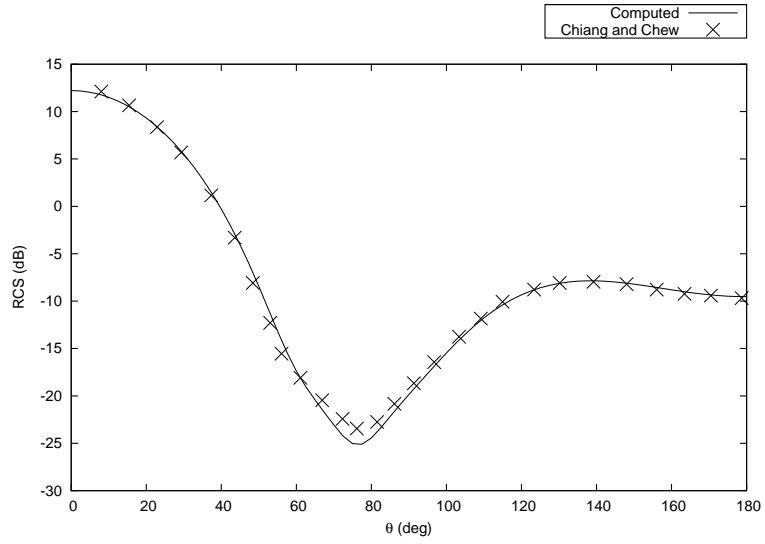


Figure 2.9: Bistatic RCS at  $\phi = 0^0$  by a dielectric sphere with radius = 1.0 m and thickness = 0.05 m with  $\epsilon_r = 2.6$  and an incident wave from  $(\theta, \phi) = (180^0, 0^0)$  at 0.2 Ghz with  $E_\theta = \eta$

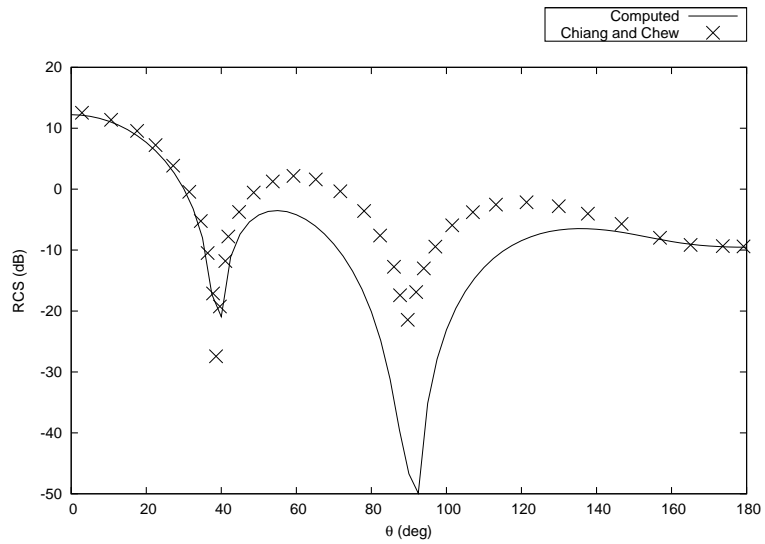


Figure 2.10: Bistatic RCS at  $\phi = 90^0$  by a dielectric sphere with radius = 1.0 m and thickness = 0.05 m with  $\epsilon_r = 2.6$  and an incident wave from  $(\theta, \phi) = (180^0, 0^0)$  at 0.2 Ghz with  $E_\theta = \eta$

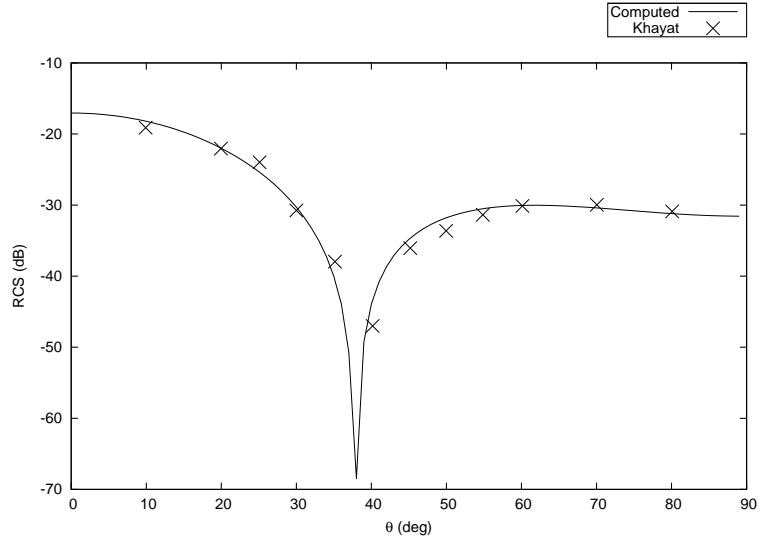


Figure 2.11: Monostatic RCS at  $\phi = 0^0$  by a homogeneous dielectric square with dimension 10.16 cm x 10.16 cm x 0.00635 cm with  $\epsilon_r = 4$  and an 2.4 GHz incident wave with  $E_\phi = \eta$  (TE polarization)

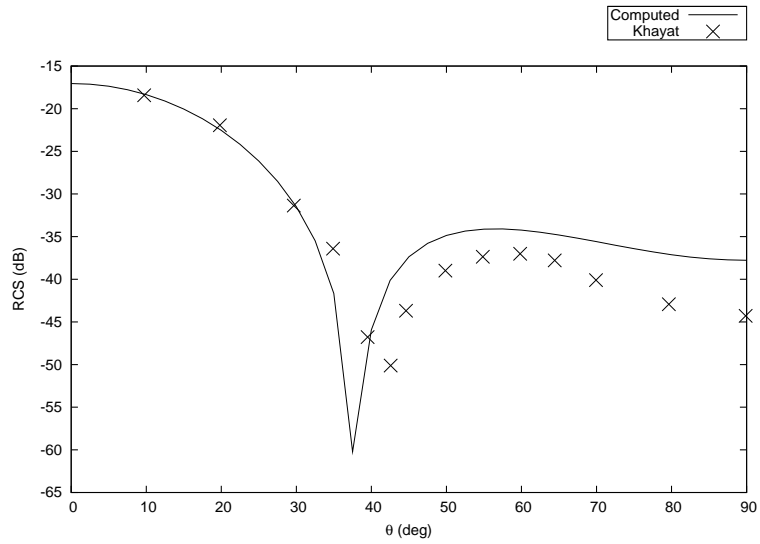


Figure 2.12: Monostatic RCS at  $\phi = 0^0$  by a homogeneous dielectric square with dimension 10.16 cm x 10.16 cm x 0.00635 cm with  $\epsilon_r = 4$  and an 2.4 GHz incident wave with  $H_\phi = 1$  (TM polarization)

## CHAPTER 3

### COMBINED PEC/THIN DIELECTRIC

In Chapter 2 a MoM formulation was developed for thin dielectric sheets. In this chapter, we will add support for perfect electric conductors (PECs) of arbitrary shape. In section 3.1, we apply the boundary conditions for the electric field on the conducting surface to obtain an integral equation for the PEC. Using this result and the integral equation developed in Chapter 2, we arrive at a pair of coupled integral equations for the combined system.

In sections 3.2 and 3.3, we apply the MoM procedure to develop a linear system where the dielectric terms from Chapter 2 appear as a submatrix to the new system. Furthermore, the coupling terms that arise from including the PEC turn out to be very similar to terms in the dielectric formulation. Thus, the codes can be combined with little extra effort.

#### 3.1 Electric Field Integral Equation - EFIE

The dielectric code can easily be expanded to incorporate perfect electrical conductors (PECs). Again, the scattered field is related to the scalar and vector potentials by:

$$\mathbf{E}^s(\mathbf{r}) = -j\omega\mathbf{A}(\mathbf{r}) - \nabla\Phi(\mathbf{r}) \quad (3.1)$$



For a PEC, the total electric field tangential to the surface is zero. This leads to the boundary condition for the PEC:

$$\mathbf{E}_{tan}^i(\mathbf{r}) = -\mathbf{E}_{tan}^s(\mathbf{r}), \mathbf{r} \in S_c \quad (3.2)$$

where  $S_c$  is the conductor surface. Substituting for the scattered field we get the desired integral equation:

$$\mathbf{E}^i(\mathbf{r})_{tan} = [j\omega\mathbf{A}(\mathbf{r}) + \nabla\Phi(\mathbf{r})]_{tan} \quad (3.3)$$

Combining this with the boundary conditions for the dielectric, we arrive at a pair of coupled equations.

$$\begin{aligned} \mathbf{E}^i(\mathbf{r})_{tan} &= [j\omega\mathbf{A}(\mathbf{r}) + \nabla\Phi(\mathbf{r})]_{tan}, \mathbf{r} \in S_c \\ \mathbf{E}^i(\mathbf{r}) &= \frac{\mathbf{J}^d}{\Omega}(\mathbf{r}) + j\omega\mathbf{A}(\mathbf{r}) + \nabla\Phi(\mathbf{r}), \mathbf{r} \in V_d \end{aligned} \quad (3.4)$$

where  $S_c$  represents the conductor surface and  $V_d$  the volume of the dielectric. Here the magnetic vector potential  $\mathbf{A}$  is generated by the currents on both the dielectric and conductor. Let  $\mathbf{A}_c$  be the vector potential due to the PEC,  $\mathbf{A}_p$  be due to the currents tangential to the surface of the dielectric, and  $\mathbf{A}_q$  the potential due to currents normal to the surface of the dielectric. The total vector potential is then:

$$\mathbf{A} = \mathbf{A}_c + \mathbf{A}_p + \mathbf{A}_q \quad (3.5)$$

The total scalar potential is defined similarly:

$$\Phi = \Phi_c + \Phi_p + \Phi_q \quad (3.6)$$

The PEC magnetic vector potential  $\mathbf{A}_c$  and scalar potential  $\Phi_c$  are given by

$$\mathbf{A}_c(\mathbf{r}) = \mu \int_{S_c} \mathbf{J}_c(\mathbf{r}') G(\mathbf{r}, \mathbf{r}') dS' \quad (3.7)$$

$$\Phi_c(\mathbf{r}) = \frac{-1}{j\omega\epsilon} \int_{S_c} \nabla \cdot \mathbf{J}_c(\mathbf{r}') G(\mathbf{r}, \mathbf{r}') dS' \quad (3.8)$$

and the potentials due to the currents in the dielectric are the same as those given in Chapter 2.

### 3.2 Current Expansion

We define a set of basis functions to approximate the current on the PEC. Let  $\mathbf{f}_n$  for  $n = 1, \dots, N_c$  be basis defined on the surface of the conductor. The total current on the conductor is then given by:

$$\mathbf{J}_c = \sum_{n=1}^{N_c} \alpha_n \mathbf{f}_n(\mathbf{r}) \quad (3.9)$$

We use RWG basis functions for the conductor. They are defined as:

$$\mathbf{f}_n(\mathbf{r}) = \begin{cases} \frac{l_n}{2A_n^+} \rho_n^+, & \mathbf{r} \in T_n^+ \\ \frac{l_n}{2A_n^-} \rho_n^-, & \mathbf{r} \in T_n^- \\ 0, & \text{otherwise} \end{cases} \quad (3.10)$$

Substituting (3.9) into (3.5) and (3.6) we get:

$$\mathbf{A} = \sum_{n=1}^{N_p} \alpha_n \mathbf{A}_{p,n} + \sum_{n=1}^{N_q} \beta_n \mathbf{A}_{q,n} + \sum_{n=1}^{N_c} \gamma_n \mathbf{A}_{c,n} \quad (3.11)$$

and

$$\Phi = \sum_{n=1}^{N_p} \alpha_n \Phi_{p,n} + \sum_{n=1}^{N_q} \beta_n \Phi_{q,n} + \sum_{n=1}^{N_c} \gamma_n \Phi_{c,n} \quad (3.12)$$

where

$$\mathbf{A}_{c,n}(\mathbf{r}) = \mu \int_{S_c} \mathbf{f}_n(\mathbf{r}') G(\mathbf{r}, \mathbf{r}') dS' \quad (3.13)$$

$$\Phi_{c,n}(\mathbf{r}) = \frac{-1}{j\omega\epsilon} \int_{S_c} \nabla \cdot \mathbf{f}_n(\mathbf{r}') G(\mathbf{r}, \mathbf{r}') dS' \quad (3.14)$$

and the remaining terms are the same as those given in Chapter 2.

### 3.3 Testing Procedure

Both sides of the equations in (3.4) are tested using the Galerkin procedure. For testing on the PEC structure we use the inner product

$$\langle \mathbf{f}, \mathbf{g} \rangle \equiv \int \mathbf{f} \cdot \mathbf{g} dS \quad (3.15)$$

in order to generate a matrix equation

$$\begin{bmatrix} Z_{cc} & Z_{cp} & Z_{cq} \\ Z_{pc} & Z_{pp} & Z_{pq} \\ Z_{qc} & Z_{qp} & Z_{qq} \end{bmatrix} \begin{bmatrix} I_c \\ I_p \\ I_q \end{bmatrix} = \begin{bmatrix} V_c \\ V_p \\ V_q \end{bmatrix} \quad (3.16)$$

which can be solved by matrix inversion.  $Z_{pp}$ ,  $Z_{pq}$ ,  $Z_{qp}$ , and  $Z_{qq}$  are the same as those given in chapter 2. The remaining submatrices are given by:

$$Z_{cc,mn} = j\omega \langle \mathbf{A}_{c,n}, \mathbf{f}_m \rangle + \langle \nabla \Phi_{c,n}, \mathbf{f}_m \rangle \quad (3.17)$$

$$Z_{cp,mn} = j\omega \langle \mathbf{A}_{p,n}, \mathbf{f}_m \rangle + \langle \nabla \Phi_{p,n}, \mathbf{f}_m \rangle \quad (3.18)$$

$$Z_{cq,mn} = j\omega \langle \mathbf{A}_{q,n}, \mathbf{f}_m \rangle + \langle \nabla \Phi_{q,n}, \mathbf{f}_m \rangle \quad (3.19)$$

$$Z_{pc,mn} = j\omega \langle \mathbf{A}_{c,n}, \mathbf{P}_m \rangle + \langle \nabla \Phi_{c,n}, \mathbf{P}_m \rangle \quad (3.20)$$

$$Z_{qc,mn} = j\omega \langle \mathbf{A}_{c,n}, \mathbf{Q}_m \rangle + \langle \nabla \Phi_{c,n}, \mathbf{Q}_m \rangle \quad (3.21)$$

and the excitation vector by:

$$V_{c,m} = \langle \mathbf{E}^i, \mathbf{f}_m \rangle \quad (3.22)$$

Now we evaluate terms given by testing on the conductor:

$$\begin{aligned} \langle \{ \mathbf{A}_{c/p/q,n} \}, \mathbf{f}_m \rangle &= \frac{l_m}{2} \left[ \{ \mathbf{A}_{c/p/q,n}(\mathbf{r}_m^{ct+}) \} \cdot \rho_m^{ct+} \right. \\ &\quad \left. + \{ \mathbf{A}_{c/p/q,n}(\mathbf{r}_m^{ct-}) \} \cdot \rho_m^{ct-} \right] \end{aligned} \quad (3.23)$$

$$\langle \nabla \Phi_{c/p/q,n}, \mathbf{f}_m \rangle = -l_m \left[ \Phi_{c/p/q,n}(\mathbf{r}_m^{c+}) - \Phi_{c/p/q,n}(\mathbf{r}_m^{c-}) \right] \quad (3.24)$$

For the dielectric testing, conductor source terms we have

$$\begin{aligned} \langle \{\mathbf{A}_{c,n}\}, \mathbf{P}_m \rangle &= \frac{l_m}{2} \tau \left[ \left( \frac{\varepsilon_{r,m}^+ - 1}{\varepsilon_{r,m}^+} \right) \{\mathbf{A}_{c,n}(\mathbf{r}_m^{ct+})\} \cdot \rho_m^{ct+} \right. \\ &\quad \left. + \left( \frac{\varepsilon_{r,m}^- - 1}{\varepsilon_{r,m}^-} \right) \{\mathbf{A}_{c,n}(\mathbf{r}_m^{ct-})\} \cdot \rho_m^{ct-} \right] \end{aligned} \quad (3.25)$$

$$\langle \nabla \Phi_{c,n}, \mathbf{P}_m \rangle = -l_m \tau \left[ \left( \frac{\varepsilon_{r,m}^+ - 1}{\varepsilon_{r,m}^+} \right) \Phi_{c,n}(\mathbf{r}_m^{c+}) - \left( \frac{\varepsilon_{r,m}^- - 1}{\varepsilon_{r,m}^-} \right) \Phi_{c,n}(\mathbf{r}_m^{c-}) \right] \quad (3.26)$$

where we have tested using the tangential currents on the dielectric. For normal component testing on the dielectric we have

$$\langle \mathbf{A}_{c,n}, \mathbf{Q}_m \rangle = \tau A_m \mathbf{A}_{c,n}(\mathbf{r}_m^{ct}) \cdot \hat{n}_m \quad (3.27)$$

$$\langle \nabla \Phi_{c,n}, \mathbf{Q}_m \rangle = \tau A_m \left( \frac{\Phi_{c,n}(\mathbf{r}_m^{ct} + 0.25\tau \hat{n}_m) - \Phi_{c,n}(\mathbf{r}_m^{ct} - 0.25\tau \hat{n}_m)}{0.5\tau} \right) \quad (3.28)$$

The coupling terms due to conductor source/testing are of the same form (within a constant multiple) of the terms in the dielectric formulation. They correspond as follows:

$$\begin{aligned} Z_{cc} &\iff Z_{pp} \\ Z_{cp} &\iff Z_{pc} \iff Z_{pp} \\ Z_{qc} &\iff Z_{qp} \\ Z_{cq} &\iff Z_{pq} \end{aligned} \quad (3.29)$$

These relationships can be very helpful when programming the combined code.

### 3.4 Numerical Results

In this section, the return loss is given for a patch antenna with a homogeneous dielectric substrate. The antenna has a 3.0 in x 2.4 in ground plane and a 1.8 in x 1.2 in patch. The dielectric has a thickness of 0.15 in and  $\epsilon_r = 5.7$ . The excitation pin is given by a flat conducting strip with a width of 0.03 in. The geometry is shown in Figure 3.1. The return loss is calculated by using the procedure in Appendix A.2 to solve for the input impedance and is matched to a  $50 \Omega$  feed.

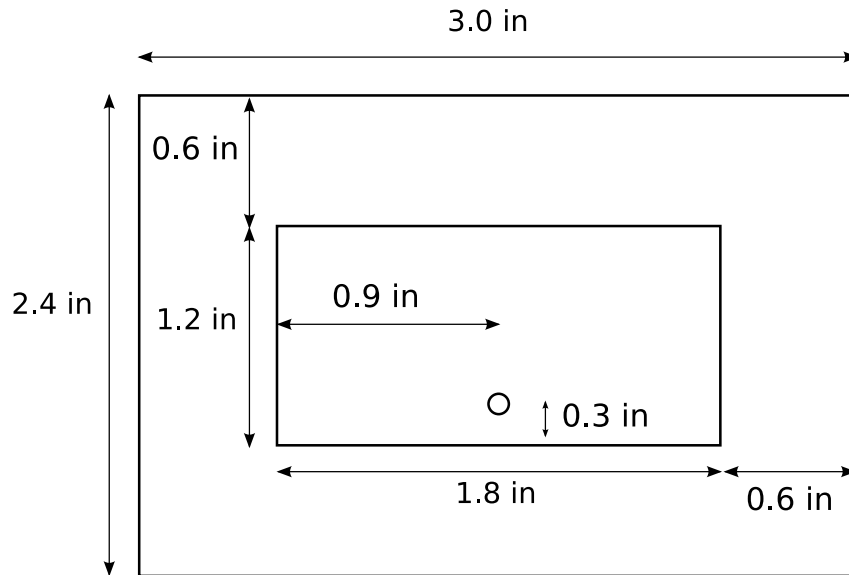


Figure 3.1: Geometry for patch antenna.

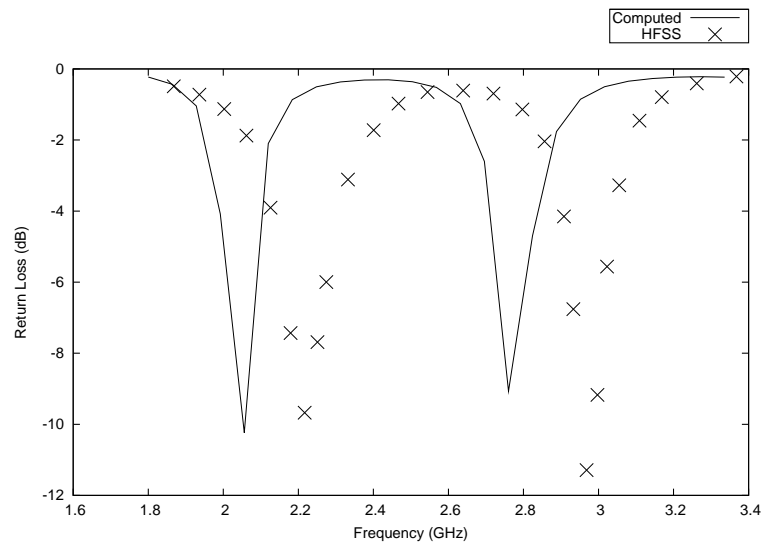


Figure 3.2: Return loss by patch antenna with homogeneous dielectric with  $\epsilon_r = 5.7$  and thickness = 0.15 in. The ground plane has dimensions 3.0 in x 2.4 in. The patch has dimensions 1.8 in x 1.2 in.

## CHAPTER 4

### CONCLUSIONS

In this work, an efficient numerical technique for modeling thin dielectric sheets in the frequency domain was developed. The dielectric is a thin sheet with constant thickness and arbitrary curvature. Furthermore, it may be either homogeneous or inhomogeneous. It was represented by a two-dimensional triangular mesh resulting in much fewer unknowns and an easier meshing process than volume formulations.

In Chapter 2, the dielectric was replaced by a set of equivalent currents. These currents were then related to the incident field using an EFIE approach. Next, the tangential currents were represented by a set of RWG basis functions while the normal component was represented by a set of pulse functions. These bases allow accurate modeling of currents within the dielectric as well as charges accumulating on the surface. Furthermore, due to the dielectric being thin, all integrals in the formulation were reduced to surface integrals greatly increasing the numerical efficiency.

In Chapter 3, the dielectric code was combined with an arbitrarily shaped conductor formulation resulting in a pair of coupled integral equations. Due to the similarity in the formulations, the conducting code was shown to be easily incorporated with the dielectric code. The validity of this formulation was demonstrated by calculating the resonances for a patch antenna.



Further research may be done in this area to extend the formulation's capabilities to multiple dielectric layers. This analysis could prove useful for thicker dielectrics where volume formulations become much more inefficient.

## BIBLIOGRAPHY

- [1] S.M. Rao, D.R. Wilton, and A.W. Glisson, "Electromagnetic scattering by surfaces or arbitrary shape," *IEEE Trans. Antennas Propag.*, vol. 30, pg 409-418, May 1982.
- [2] I.T. Chiang and W.C. Chew, "Thin dielectric sheet simulation by surface integral equation using modified RWG and pulse bases," *IEEE Trans. Antennas Propag.*, vol. 54, pg 1927-1934, Jul. 2006.
- [3] I.T. Chiang and W.C. Chew, "A Coupled PEC-TDS Surface Integral Equation Approach for Electromagnetic Scattering and Radiation From Composite Metallic and Thin Dielectric Objects," *IEEE Trans. Antennas Propag.*, vol. 54, pg 3511, Jul. 2006.
- [4] R.F. Harrington, *Field Computation by Moment Methods*. New York: IEEE Press, 1993.
- [5] S.M. Rao, "Electromagnetic Scattering and Radiation of Arbitrarily-Shaped Surfaces by Triangular Patch Modeling," Ph.D. Dissertation University of Mississippi, Aug. 1980.
- [6] Shian-Uei Hwu, "Electromagnetic Modeling of Conducting and Dielectric Coated Wire, Surface, and Junction Configurations," Ph.D. Dissertation University of Houston, May 1990.
- [7] Michael A. Khayat, "Numerical Modeling of Thin Materials in Electromagnetic Scattering Problems," Ph.D. Dissertation University of Houston, Dec. 2003.
- [8] D. Schaubert, D. Wilton, and A. Glisson, "A tetrahedral modeling method for electromagnetic scattering by arbitrarily shaped inhomogeneous dielectric bodies," *IEEE Trans. Antennas Propag.*, vol. 32, pg 77-85, Jan. 1984.

APPENDIX A  
NUMERICAL RESULTS

**A.1 RCS**

Once we have solved for the currents on a given structure, we may calculate its radar cross section (RCS) given by the quantity

$$\sigma = \lim_{r \rightarrow \infty} 4\pi r^2 \frac{|\mathbf{E}^s|^2}{|\mathbf{E}^i|^2} \quad (\text{A.1})$$

where  $\mathbf{E}^i$  is the incident field and  $\mathbf{E}^s$  is the scattered field calculated in the far-field in the direction of

$$\hat{\mathbf{r}} = \sin \theta \cos \phi \hat{\mathbf{x}} + \sin \theta \sin \phi \hat{\mathbf{y}} + \cos \theta \hat{\mathbf{z}} \quad (\text{A.2})$$

The far field is given by:

$$\mathbf{E}^s = -j\omega \mathbf{A} = -j\omega \mu \int \mathbf{J} \frac{e^{-jkR}}{4\pi R} dv' \quad (\text{A.3})$$

If we let  $\mathbf{r}'$  be the integration coordinates, then as  $r \rightarrow \infty$  we can approximate  $R$  as

$$R = \frac{(\mathbf{r} - \mathbf{r}') \cdot (\mathbf{r} - \mathbf{r}')}{|\mathbf{r} - \mathbf{r}'|} \approx r - \hat{\mathbf{r}} \cdot \mathbf{r}' \quad (\text{A.4})$$

giving us

$$\mathbf{E}^s \approx \frac{-j\omega \mu}{4\pi r} e^{-jkr} \int \mathbf{J} e^{jk\hat{\mathbf{r}} \cdot \mathbf{r}'} dv' \quad (\text{A.5})$$

Using this approximation we can calculate the far-field contributions given by the currents on the dielectric ( $\mathbf{E}_p^s$  and  $\mathbf{E}_q^s$ ) as well as the conductor ( $\mathbf{E}_c^s$ ). We approximate each basis function at the centroid of the corresponding triangle(s). For the tangential component on the dielectric sheet we have

$$\mathbf{E}_p^s = \frac{-j\omega\mu\tau}{8\pi r} e^{-jkr} \sum_{n=1}^{N_p} \alpha_n l_n \left[ \left( \frac{\varepsilon_{r,n}^+ - 1}{\varepsilon_{r,n}^+} \right) \rho_n^{ct+} e^{jk\hat{\mathbf{r}} \cdot \mathbf{r}_n^{ct+}} \right. \quad (\text{A.6})$$

$$\left. + \left( \frac{\varepsilon_{r,n}^- - 1}{\varepsilon_{r,n}^-} \right) \rho_n^{ct-} e^{jk\hat{\mathbf{r}} \cdot \mathbf{r}_n^{ct-}} \right] \quad (\text{A.7})$$

and for the normal component:

$$\mathbf{E}_q^s = \frac{-j\omega\mu\tau}{4\pi r} e^{-jkr} \sum_{n=1}^{N_q} \beta_n A_n e^{jk\hat{\mathbf{r}} \cdot \mathbf{r}_n^{ct}} \quad (\text{A.8})$$

Similarly the scattered field from the conductor is given by:

$$\mathbf{E}_c^s = \frac{-j\omega\mu}{8\pi r} e^{-jkr} \sum_{n=1}^{N_c} \gamma_n l_n \left[ \rho_n^{ct+} e^{jk\hat{\mathbf{r}} \cdot \mathbf{r}_n^{ct+}} + \rho_n^{ct-} e^{jk\hat{\mathbf{r}} \cdot \mathbf{r}_n^{ct-}} \right] \quad (\text{A.9})$$

where  $\alpha_n$ ,  $\beta_n$ , and  $\gamma_n$  are the magnitudes for  $\mathbf{P}_n$ ,  $\mathbf{Q}_n$ , and  $\mathbf{f}_n$  respectively.

## A.2 Antenna Input Impedance

Another problem of practical importance is calculating the input impedance of an antenna. In order to do this we use the delta-gap feed model. An E-field is applied to a junction between two triangles such that a constant voltage is maintained across an infinitesimal gap where the triangles join. We define  $E^i = V$  across the gap and

$E^i = 0$  otherwise. The field is oriented in the same direction as the basis  $\mathbf{f}_m$  connecting the two triangles. Testing provides us with the excitation

$$V_{c,m} = \int \mathbf{E}^i \cdot \mathbf{f}_m dS = V \int dl = Vl_m \quad (\text{A.10})$$

If  $I_m$  is the coefficient for  $\mathbf{f}_m$ , the total current across the gap is  $l_m I_m$ . The input impedance is then calculated by

$$Z_{in} = \frac{V}{l_m I_m} \quad (\text{A.11})$$

For a  $50 \Omega$  feed line, the reflection coefficient is given by:

$$\Gamma_L = \frac{Z_{in} - 50}{Z_{in} + 50} \quad (\text{A.12})$$

The return loss is then calculated by:

$$RL = 20 \log |\Gamma_L| \quad (\text{A.13})$$

### A.3 A Note On Dielectric Meshing Requirements

It should be noted that increasing the relative permittivity of a dielectric also increases the electrical size of the material. The typical meshing recommendation for a surface is 100 divisions/square wavelength (defining electrically small as less than

a tenth of a wavelength). The wavelength in a dielectric is given by

$$\lambda_G = \frac{c_o}{f\sqrt{\varepsilon_r}} \quad (\text{A.14})$$

where  $c_o$  is the speed of light in free space and  $\varepsilon_r$  is the relative permittivity of the dielectric material. This implies  $\lambda_G^2 = \frac{\lambda_o^2}{\varepsilon_r}$  where  $\lambda_o$  is the wavelength in free space for the frequency of interest. In other words, the meshing requirement increases linearly with the relative permittivity of the material. This results in a large increase in unknowns for problems involving dielectrics with large  $\varepsilon_r$ .